


Extending Stable Parameter Range of LCL- filters for Grid-Connected Converters by Inherent Damping of Model Predictive Control (MPC)

Conference Paper**Author(s):**

Jeong, Min; Gfrörer, Tino; Biela, Jürgen 

Publication date:

2022

Permanent link:

<https://doi.org/10.3929/ethz-b-000564410>

Rights / license:

[In Copyright - Non-Commercial Use Permitted](#)

Originally published in:

<https://doi.org/10.1109/compel53829.2022.9829978>

Extending Stable Parameter Range of LCL-filters for Grid-Connected Converters by Inherent Damping of Model Predictive Control (MPC)

Min Jeong

High Power Electronic Systems (HPE)
ETH Zürich
jeong@hpe.ee.ethz.ch

Tino Gfrörer

High Power Electronic Systems (HPE)
ETH Zürich
tinog@student.ethz.ch

Jürgen Biela

High Power Electronic Systems (HPE)
ETH Zürich
jbiela@ethz.ch

Abstract—Conventional linear controllers with active damping (AD) cannot stabilise LCL-filters for certain ranges of filter parameters due to resonances. This limits the design space of the filter design and can lead to sub-optimal designs in terms of filter volume and efficiency. When model predictive control (MPC) with a long-prediction horizon is applied, the inherent damping capability of MPC can stabilise the system despite the resonance phenomenon and expands the design space. In this paper, the limited design space due to insufficient damping of linear controllers with AD is analyzed based on capacitor current feedback AD. Exemplary LCL-filter optimization solutions and the resulting Pareto fronts are presented to illustrate the achievable volume and/or loss reductions with the extended design space. A novel MPC formulation is proposed to adopt explicit MPC and to enable a real-time implementation even at a high switching frequency. Simulation results validate the presented analysis.

Index Terms—Continuous control set (CCS) MPC, Design parameter space extension, LCL-filter damping, Optimal system design, Explicit MPC

I. INTRODUCTION

LCL-filters attenuate high-frequency harmonics generated by switching operations of pulse width modulation voltage-source converters (VSCs) and are gaining attention due to their compact size and improved dynamic performance [1], [2]. However, LCL-filter resonance may amplify unwanted harmonics and can negatively affect the closed-loop control performance, which can even lead to instability. Therefore, a VSC with an LCL-filter is typically controlled by a classic linear controller with an extra damping loop for ensuring the system stability. Extensive research has been conducted for different active damping (AD) methods, because of the higher power densities [3], [4].

However, AD methods do not only require additional control effort for properly damping the system resonance, but also complicate the LCL-filter design process, since classical linear controllers with AD often cannot stabilise the system or provide sufficient damping in certain cases. For example, [4] investigates the most widely used AD method of the capacitor current feedback approach and demonstrates that the controller cannot stabilise the system when the resonance frequency of the LCL-filter is around one-sixth of the sampling

frequency ($f_s/6$), named the critical resonance frequency f_{cri} . This limits the possible parameter space of the LCL-filter (i.e. the $L_{fi}/C_f/L_{fg}$ values) and results in a design either with an undesired high switching frequency or a relatively large inductance value, which leads to higher losses or bigger filter components [2].

A general stability of LCL-filters without limitations of the parameter range can be achieved with advanced control schemes as for example model predictive control (MPC). MPC has attracted attention as an alternative control method because it can overcome shortcomings of classical control methods [5]. When MPC with a long-prediction horizon is applied, the resonance of the system is predicted and the control laws resulting from solutions of optimization problems have inherent damping capability without extra passive components or additional damping loops [6]. Therefore, MPC can stabilise LCL-filters with sufficient damping even when the filter resonance frequency is close to the critical resonance frequency f_{cri} . However, it has not been investigated how MPC can be used to extend the possible filter design space and to further optimize the filter design. Furthermore, a real-time implementation of MPC with a long-prediction horizon is still challenging. Experimental demonstrations shown in [6] and [7] are limited to low switching frequencies. This hinders practical application of CCS-MPC despite its merits, since many new applications like active power filter [8] or systems using wide-bandgap semiconductors [9] beneficially operate at high switching frequencies.

This paper proposes a novel MPC formulation to adopt explicit MPC, such that the benefit of MPC can be used even at high switching frequencies. Based on the proposed MPC, the impact of the inherent damping capability of MPC on an LCL-filter design is investigated. With MPC, a wider range of LCL-filter parameters ($L_{fi}/C_f/L_{fg}$) can be used for given system-level specifications so that a more compact and efficient system design is possible. The analysis is exemplarily conducted for a grid-connected VSC with an LCL-filter, but it can be also applied to multi-level VSCs or other applications like active power filters.

This paper is organized as follows: First, LCL-filter models are briefly explained in section II. Section III presents a

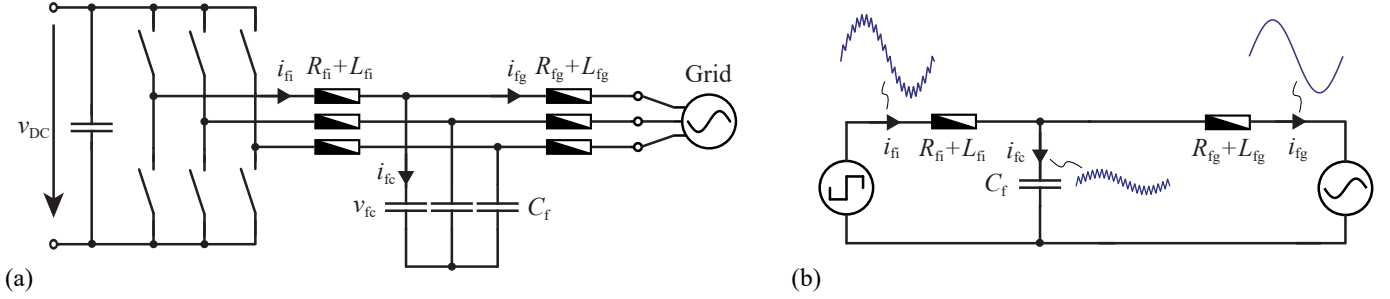


Fig. 1. (a) Three-phase two-level grid-connected VSC with an LCL-filter. (b) Equivalent per-phase model with ideal current waveforms.

novel MPC formulation to apply explicit MPC. Section IV investigates the design space based on the damping capability and section V demonstrates the impact on the optimal filter design. Finally, in section VI, simulation results are shown to verify and analyze the control performance of the proposed MPC.

II. LCL-FILTER MODEL

A typical three-phase two-level converter connected to the grid through an LCL-filter is shown in fig. 1(a). The LCL-filter can be modeled in two ways, in frequency-domain and in time-domain. Transfer functions in the frequency-domain can effectively characterize resonances of the filter and reveals the attenuation of switching harmonics by the filter. Therefore, the model is used in section IV-B for designing the filter to achieve a required attenuation level by the grid-side LC-filter. In contrast, a state-space representation in time-domain is better for describing the instantaneous system dynamics, so the model is used in section III-A for predicting future plant behaviors in the proposed MPC formulation. The two models are briefly reviewed in this section.

A. Transfer Function

If all parasitic resistors are neglected for simplicity, two transfer functions of the LCL-filter can be written in the s -domain

$$G_1(s) = \left. \frac{i_{fg}}{v_i} \right|_{v_g=0} = \frac{1}{(L_{fi}L_{fg}C_f)s^3 + (L_{fi} + L_{fg})s} \quad (1)$$

$$G_2(s) = \left. \frac{i_{fg}}{i_{fi}} \right|_{v_g=0} = \frac{1}{(L_{fg}C_f)s^2 + 1} \quad (2)$$

as shown in [1], and the resonance frequency of the LCL-filter is given by

$$f_{res} = \frac{1}{2\pi} \sqrt{\frac{L_{fi} + L_{fg}}{L_{fi}L_{fg}C_f}}. \quad (3)$$

The converter output voltage is considered to be a sinusoidal voltage source for such harmonic component for deriving $G_1(s)$, while describing the frequency characteristics of the complete LCL-filter. The converter output current is considered to be a sinusoidal current source for such harmonic component for deriving $G_2(s)$, while describing the frequency characteristics of the grid-side LC-filter. In section IV-B, the

grid-side inductance value can simply be calculated with $G_2(s)$ based on a converter-side current ripple and a required attenuation level by the grid-side LC-filter.

B. State-space Representation

The dynamics of the LCL-filter can be described in the $\alpha\beta$ -reference frame and a continuous time-domain state-space representation of the system is defined based on [7], [10] as

$$\frac{d}{dt}\mathbf{x} = \mathbf{F}\mathbf{x} + \mathbf{G}\mathbf{s}_{abc} + \mathbf{P}\mathbf{v}_{g,\alpha\beta}, \quad (4)$$

where $\mathbf{x} = [i_{fi,\alpha} \ i_{fi,\beta} \ v_{fc,\alpha} \ v_{fc,\beta} \ i_{fg,\alpha} \ i_{fg,\beta}]^T$ is the state vector, $\mathbf{s}_{abc} \in \{-1, 1\}^3$ is the three-phase PWM signal, and $\mathbf{v}_{g,abc}$ is the three-phase grid voltage. The detailed equations and matrices are given in [7], [10]. The control input vector \mathbf{s}_{abc} is represented in the abc -frame, since it allows formulating input constraints in MPC with simple box-constraints. In the $\alpha\beta$ -frame, the input constraints have the shape of a hexagon and consequently require a complex polytopic formulation. Based on the explained state-space representation model, a novel MPC formulation is proposed in the following section.

III. MODEL PREDICTIVE CONTROL (MPC)

Many MPC concepts have been proposed for controlling VSCs with LCL-filters [6], [7], [11], [12], which can be split in two groups: Finite control set MPC (FCS-MPC) and continuous control set MPC (CCS-MPC). FCS-MPC determines switching actions directly without a modulator and is widely applied in power electronics due to its simplicity. However, a long-prediction horizon is generally not feasible for FCS-MPC as the computational burden of the integer optimization problem of FCS-MPC grows exponentially with the prediction horizon. On the other hand, CCS-MPC usually has a convex underlying optimization problem, which is more scalable for long-prediction horizons that have inherent damping capability [6]. Nonetheless, a real-time implementation of CCS-MPC with a long-prediction horizon is still challenging [6] and [7].

Explicit MPC (EMPC) can enable a real-time implementation of CCS-MPC at fast sampling rates, since EMPC solves the optimization problem of CCS-MPC off-line and only performs relatively simple on-line computations. However, when the problem size of CCS-MPC grows, i.e. systems with many states and/or inequality constraints are considered, the number of generated regions in EMPC often grows exponentially and

the memory requirement becomes problematic. The move-blocking method is often used for limiting the number of generated regions with EMPC as shown in [12], but this method does not describe the achievable dynamics of the system correctly because the control input varies abruptly, when MPC is designed to have a dead-beat behavior.

In order to overcome the mentioned limitations, a MPC formulation is proposed in the following section, such that explicit MPC can be adopted to implement MPC in real-time even for a high switching frequency operation. Furthermore, detailed results for explicit MPC including memory requirements are presented.

A. Proposed CCS-MPC Formulation

As will be shown, the standard CCS-MPC proposed in [6] and [7] can be adjusted, such that it keeps the dead-beat behavior with all constraints in the first few prediction steps and then neglects the constraints in the following steps. The control inputs during the following steps are punished indirectly by a cost function. In this way, the number of constraints can be reduced, while the benefit of damping with a long-prediction horizon can be kept.

The MPC law can be formulated as

$$\begin{aligned} \min_{\mathbf{U}_k} J \\ \text{s.t. } \mathbf{x}_{k+l+1} = \mathbf{A}\mathbf{x}_{k+l} + \mathbf{B}\mathbf{u}_{k+l}, \quad \forall l \in \mathcal{I} \quad (6a) \end{aligned}$$

$$\frac{-v_{dc}}{2} \cdot \mathbf{1}_{3 \times 1} \leq \mathbf{u}_{k+l} \leq \frac{v_{dc}}{2} \cdot \mathbf{1}_{3 \times 1}, \quad \forall l \in \mathcal{I}_{db} \quad (6b)$$

where $\mathbf{U}_k = [\mathbf{u}_k^T, \dots, \mathbf{u}_{k+N_p-1}^T]^T \in \mathbb{R}^{3 \cdot N_p}$ is the complete control input vector, J is the cost function given in (5) at the bottom of the page, N_p is the full prediction horizon, $N_{p,db}$ is the prediction horizon with constraints for a dead-beat behavior, $\mathbf{Q} \geq 0$, $\mathbf{R}_{db} \geq 0$, and $\mathbf{R} \geq 0$ are weighting matrices, $\mathcal{I} = \{0, 1, \dots, N_p - 1\}$, $\mathcal{I}_{db} = \{0, 1, \dots, N_{p,db} - 1\}$, and $\|\mathbf{z}\|_{\mathbf{Q}}^2$ denotes a 2-norm with the weighting matrix \mathbf{Q} . The equality constraints for the LCL-filter system dynamics based on (4) are given in (6a), and the input constraints based on the available DC-link voltage are given in (6b). Though only input constraints are considered in this work, state constraints on converter-side currents or on filter capacitor voltages can be also added to fully exploit inductors and/or capacitors up to their physical limits.

B. Explicit MPC (EMPC) and Real-time capability

The MPC formulation proposed in (6) can be reformulated in a condensed quadratic programming (QP) problem and further can be converted into a general multi-parametric quadratic programming (mp-QP) problem. Then, the process of solving the underlying optimization problem can be conducted off-line, resulting in a piecewise affine function of the optimization parameters. The proposed MPC formulation has a relatively

$$J = \sum_{l=0}^{N_{p,db}-1} (\|\mathbf{x}_{k+l+1} - \mathbf{x}_{ref,k+l+1}\|_{\mathbf{Q}}^2 + \|\mathbf{u}_{k+l}\|_{\mathbf{R}_{db}}^2) + \sum_{l=N_{p,db}}^{N_p-1} (\|\mathbf{x}_{k+l+1} - \mathbf{x}_{ref,k+l+1}\|_{\mathbf{Q}}^2 + \|\mathbf{u}_{k+l} - \mathbf{u}_{k+l-1}\|_{\mathbf{R}}^2) \quad (5)$$

TABLE I
IMPLEMENTATION PARAMETERS FOR EXPLICIT MPC

$N_{p,db}^a$	No. of Region	Memory Requirement	
		Region-based	Region-less
1	19	143 kB	37 kB
2	361	3216 kB	120 kB
3	6859	67.7 MB	2.37 MB
4	130,321 ^b	-	-

^a : All with the full prediction horizon (N_p) of 10

^b : Not feasible on embedded systems

low number of inequality constraints, and a long prediction horizon does not increase the complexity of the MPC. Therefore, the off-line mp-QP problem can be solved efficiently by the combinatorial method presented in [13] and results in a reasonable number of regions with EMPC.

Implementation parameters for EMPC are given in table I, where the number of the generated regions and the memory requirements of two different EMPC implementation methods for different $N_{p,db}$ values are shown. The results are based on the LCL-filter system parameters given in table II. Comparative simulation results regarding control performance with different $N_{p,db}$ values are given in section VI-C. A real-time implementation at a high switching frequency can be achieved in this size range of region numbers using an FPGA device as demonstrated in [14]. In the following section, it will be shown how the possible filter design space can be extended based on the proposed MPC.

IV. DESIGN SPACE EXTENSION WITH MPC

When an LCL-filter is designed, design requirements such as maximum inductor current ripple and allowed reactive power consumption limit the possible parameter space of the LCL-filter ($L_{fi}/C_f/L_{fg}$). The allowed parameter values for these limits result in the design space of the LCL-filter. There, an extra limitation is added when a conventional linear controller with AD is used, since the controller cannot provide sufficient damping for a range of LCL-filter parameters. With the inherent damping capability of the MPC proposed in section III, this limitation imposed due to insufficient damping of the controller can be removed. Therefore, a wider range of LCL-filter parameters can be used for the filter design. In the following, the parameter space limit due to AD is described first. Then, the conventional design space with AD and the extended design space with MPC are calculated and compared to assess the influence of the limitation removal with MPC, .

A. Parameter limit due to insufficient damping with AD

Many AD methods cannot stabilise the system or provide sufficient damping for a certain range of filter parameters.

TABLE II
LCL-FILTER SYSTEM PARAMETERS GIVEN IN [4].

Symbol	Value	Symbol	Value		
v_{dc}	DC voltage	650 V	$v_{g,rmsll}$	Grid voltage	415 V
i_{rated}	Rated current	12 A	f_{sw}	Switching frequency	5 kHz
L_{fi}	Converter-side inductance	$6 \mu\text{H}$	L_{fg}	Grid-side inductance	$2 \mu\text{H}$
C_f	Filter capacitance	$6 \mu\text{F}^a / 9 \mu\text{F}^b$	f_{res}	Resonance frequency	$1.67 \text{ kHz}^a / 1.37 \text{ kHz}^b$

^a: Parameters at the critical resonance frequency, where CCF-AD cannot stabilise the system.

^b: Parameters, where CCF-AD cannot provide sufficient damping.

For example, it has been investigated in [4] based on grid-current feedback, that the most widely used capacitor current feedback active damping (CCF-AD) cannot damp the LCL-filter system effectively if the resonance frequency f_{res} is around one-sixth of the sampling frequency ($f_s/6$), i.e. f_{cri} . In [3], similar results regarding the system stability around the critical frequency f_{cri} are demonstrated based on converter-current feedback combined with lead-lag network AD. The LCL-filter system shows either instability or underdamped step response with large overshoots if the LCL-filter is designed with the parameters around the critical resonance frequency f_{cri} . Therefore, these parameters cannot be selected and this limits the conventional design space with AD.

B. Extended design space with MPC

The limit due to insufficient damping capability of AD is analyzed based on the AD method and the parameters given in [4]. The results are given in fig. 2(a) for sweeping the parameter space of the LCL-filter ($L_{fi}/C_f/L_{fg}$) around the critical resonance frequency f_{cri} . The results are shown in three different colors depending on their damping behavior based on the relative distance $d_{rel} := |f_{res} - f_{cri}| / f_{cri}$:

- The red dots represent the parameter sets, where the resonance frequency is close ($d_{rel} \leq 5\%$) to the critical resonance frequency, such that the AD method cannot stabilise the system.

- The yellow dots represent the parameter sets, where the resonance frequency is not very close ($5\% \leq d_{rel} \leq 20\%$) to the critical resonance frequency, but the AD cannot provide sufficient damping.
- The green dots represent the parameters set, where the resonance frequency is far away ($20\% \leq d_{rel}$) from the critical frequency and the AD can provide enough damping to the system with good control performance.

When the limit due to the insufficient damping capability of AD is combined with other LCL-filter design requirements, the design space of the LCL-filter system can be determined. In the following, based on the LCL-filter design procedure proposed in [1], three design steps are used to determine the design space. First, the converter-side inductance is determined, such that the current ripple is between 5%-50% of the rated current of the system. This limits the maximum converter-side current ripple. Then, the filter capacitor is chosen between 1%-10% of the base capacitance (defined in [1]) to limit the maximum reactive power consumption. Finally, the grid-side inductance is determined, such that the current ripple is attenuated to 2% by the grid-side LC-filter. The results are given in fig. 2(b) with the same color code. The conventional design space (green dots) is limited to only green dots due to insufficient damping capability of AD. The extended design space with MPC (green/yellow/red dots) consists of all parameter sets because of the good inherent damping capability of MPC.

With MPC even parameter sets for red and yellow dots

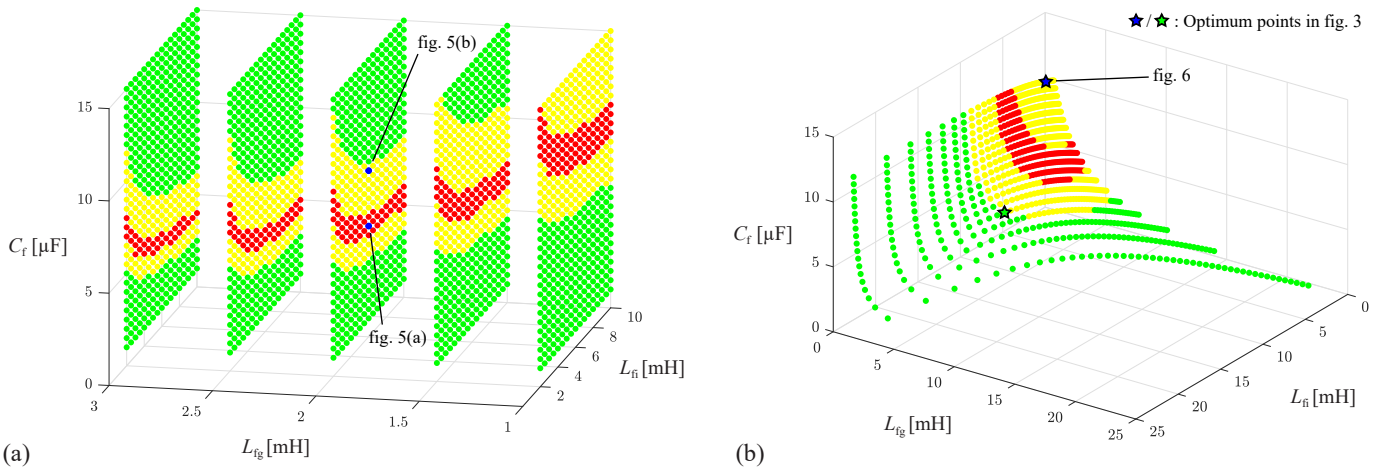


Fig. 2. (a) Limited parameter space due to insufficient damping capability of CCF-AD based on the method and the parameters given in [4]. (b) Design space of the LCL-filter with the design requirements proposed in [1]. Parameter sets, which result in the optimum points given in fig. 3 regarding the product of the volume and losses, are marked as star points.

can be selected, and an optimal system parameter design can be realized without dependency on the AD. Depending on the application, the complete converter and/or the LCL-filter design optimization can focus on different aspects and the objective can either be losses, weight, volume, or any combination of these, leading to extra requirements [8], [15].

V. IMPACT OF MPC ON OPTIMAL DESIGN

In order to demonstrate the impact of the design space extension with MPC on the optimal filter design, an exemplary optimization result for an LCL-filter design regarding volume and losses is presented in the following. The resulting two Pareto fronts, one for the conventional design space with the linear controller and one for the extended design space with the MPC, are shown. Based on the Pareto fronts, exemplary optimum design points are selected based on the product of volume and losses, and the results for these design points are compared.

In the following, first, inductor and capacitor models are discussed to effectively calculate the volume and the losses of the LCL-filter components for given LCL-filter parameter sets in fig. 2(b). Then, different designs are calculated based on commercially available core geometries, showing a trade-off between the filter volume and the losses.

A. Inductor Model

In LCL-filters, inductors typically take a considerable share of volume, weight, and losses. Therefore, both converter-side and grid-side inductors should be optimized. There, many factors (e.g. used magnetic core material or type of winding wires) need to be accounted.

Grid-side inductors conduct mainly a current at mains frequency as shown in fig. 1(b), since ripples at high harmonics are attenuated to fulfill grid code requirements at the PCC. Therefore, laminated silicon steel is selected as core material for the grid-side inductors as it features high saturation flux density and minimises the area product of the magnetic

TABLE III
STEINMETZ PARAMETERS AND SATURATION FLUX DENSITY

Materials	k	α	β	B_{sat}
Silicon Steel	4.50	1.51	1.76	2
Amorphous	2.64	1.39	1.64	1.56

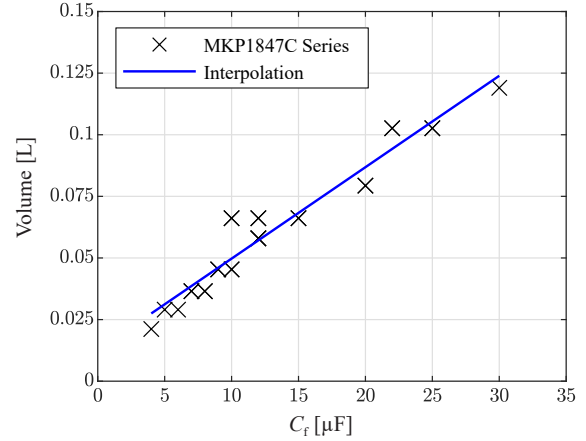


Fig. 4. Interpolated capacitor volume, as a function of the capacitance for the capacitor series MKP1847C from Vishay.

components. Round wire is used for the designs because skin and proximity losses are not high at the mains frequency.

Due to the switching operations of the converter, converter-side inductors conduct a low frequency current at mains frequency with superimposed high frequency harmonics as shown in fig. 1(b). Therefore, an amorphous material is selected for the magnetic core of the converter-side inductors to avoid high core-losses. Furthermore, litz wire is used for the designs to limit the winding losses due to high frequency current components.

The inductor losses are calculated based on the following models, which are based on [16].

1) *Core losses*: The core losses are calculated with the improved generalized Steinmetz equation (iGSE). The Steinmetz

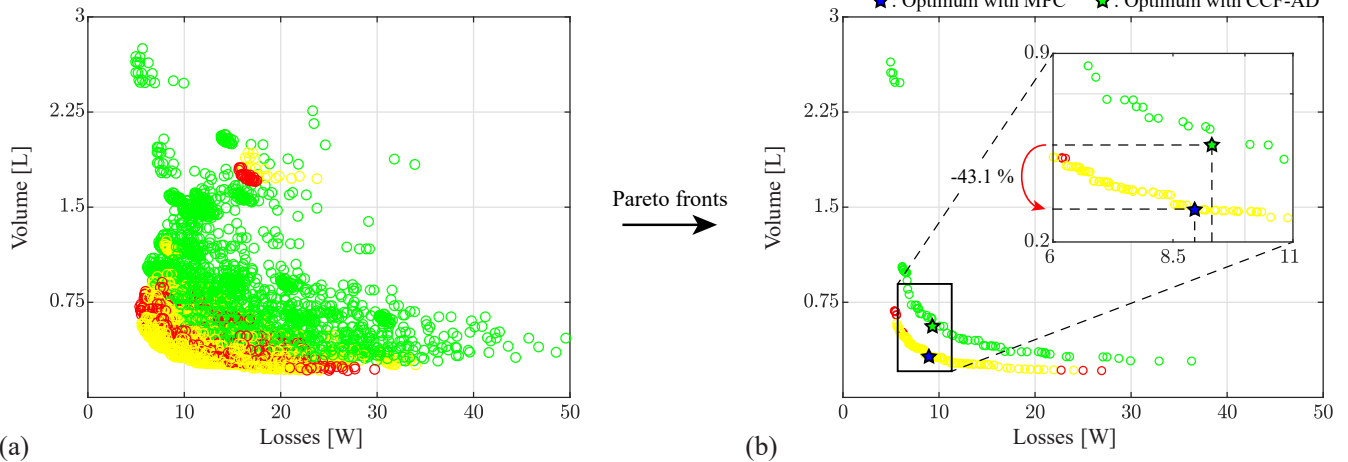


Fig. 3. LCL-filter optimization results based on the filter parameters given in fig.2(b). The results are presented with the same color code as used in fig.2(b) and can be interpreted as: The green dots (●) are the optimization results of the conventional design space with the linear controller, and all dots (●/●/●) are the optimization results with the extended design space with MPC. (a) All discovered solutions are shown. (b) Two Pareto-fronts from each design space are shown together with optimum points with respect to the product of the volume and losses.

parameters of the used magnetic core materials are given in table III.

2) *Winding losses*: The winding losses are calculated including the skin effect and the proximity effect. The mirroring method is used to calculate the H -field distribution in the core window considering also the air gaps in the cores. For the converter-side inductors, the internal proximity effect in the litz wire is also included to compute the winding losses.

Since the core geometry is required to calculate the total losses, actual core geometry data of C-cores from Nicore are used for the inductor designs. For the litz wires, four commercially available strand diameters are considered: 0.361, 0.202, 0.101, and 0.071 mm

B. Capacitor Design

In this work, film capacitors of the Vishay MKP1847C series are considered for designing the filter capacitor, because they feature low losses due to a small ESR and a small leakage current. Since the chosen film capacitor series has a very low dissipation factor ($\tan \delta$), the dielectric losses are neglected. The volume of film capacitors typically scales linearly with the capacitance, since the thickness of the dielectric layers mainly determines the capacitance. Therefore, the volume of the capacitors is estimated by interpolating the actual data of the capacitor series. The result of the interpolation is shown in fig. 4.

C. Optimization of LCL-filter

For each LCL-filter parameter set ($L_{fi}/C_f/L_{fg}$) given in fig. 2(b), many feasible solutions exist since the required inductance can be realized with different sizes of cores and numbers of turns. Therefore, an inductor optimization routine similar to [17] is used to identify the 5 best solutions resulting in the lowest product of volume and losses. The inductor optimization routine is performed for both converter-side and grid-side inductors, and the resulting 25 combinations are regarded as inductor design sets. The combinations enable illustrating a trade-off between the achievable volume and losses for each parameter set. With the estimated capacitor volume based on the required capacitance, the volume and losses of the complete LCL-filter can be determined. The LCL-filter optimization can be performed by iterating through all possible LCL-filter parameter sets.

The results of the LCL-filter optimization are shown in fig. 3(a). For each parameter set given in fig. 2(b), the achieved 25 solutions from the optimization procedure are marked in the same color code to illustrate the impact with the extended design space. In fig. 3(b), the Pareto fronts of each design space are shown for comparison. The Pareto fronts from the extended design space (marked in yellow/red) are located closer to the origin compared to the one of the conventional design space (marked in green), indicating that lower losses

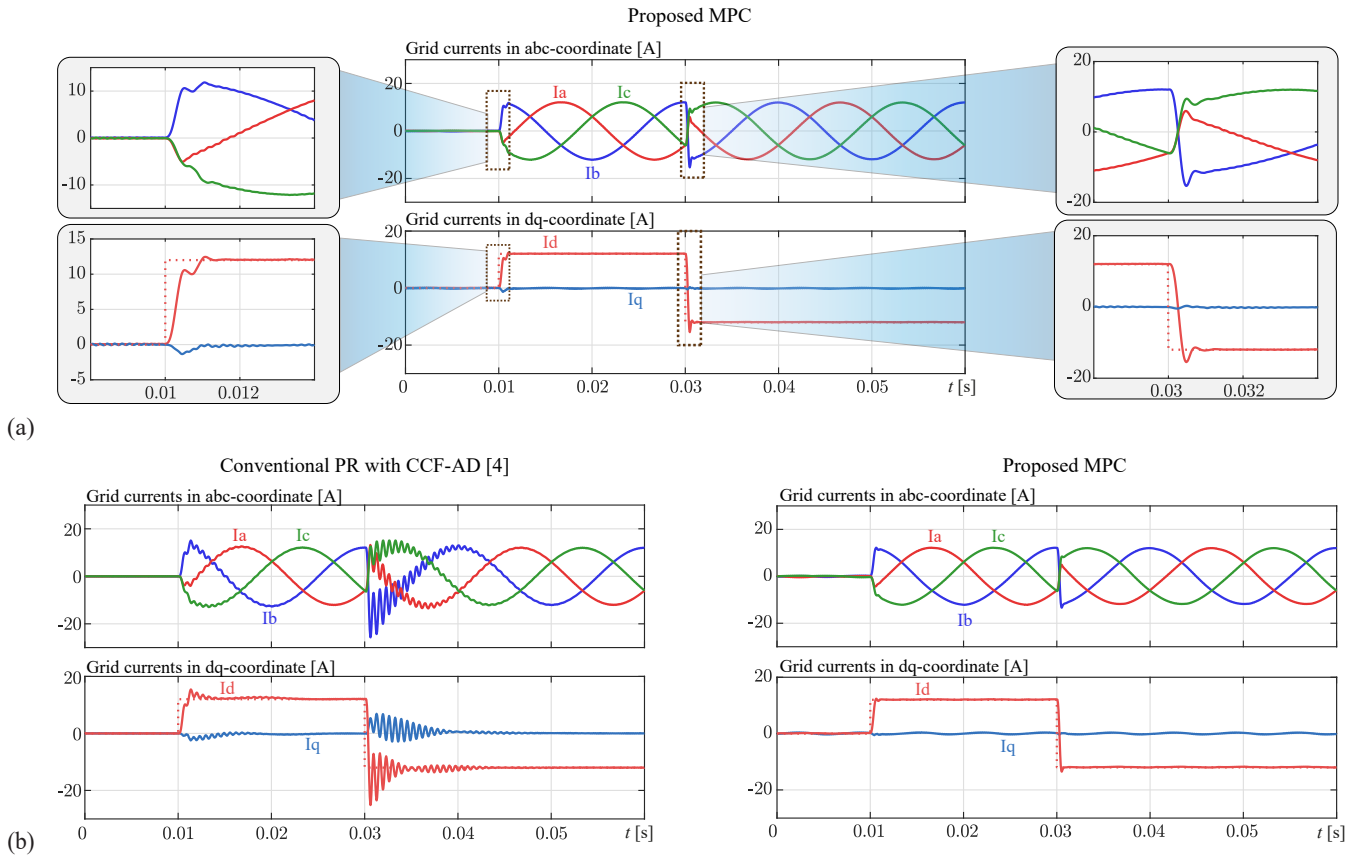


Fig. 5. Simulation results at two different parameter sets. (a) Parameter ($C_f = 6 \mu\text{F}$) at the critical resonance frequency, shown red in fig. 2(a), where linear controllers with CCF-AD cannot stabilise the system. (b) Parameter ($C_f = 9 \mu\text{F}$) at the border of the underdamped group, shown yellow in fig. 2(a), where linear controllers with CCF-AD cannot provide sufficient damping.

and/or a smaller volume can be achieved with MPC. An exemplary optimum point is marked in fig. 3 for each design space, which gives the best product of the volume and losses. A volume reduction of 43% is achieved for realizing the LCL-filter with the extended design space.

VI. SIMULATION RESULTS

In this section, comprehensive simulation results of the proposed MPC formulation are presented. First, the control performance of the MPC is evaluated with 3 different sets of LCL-filter parameters marked in fig. 2 and is compared to that of a conventional linear controller, implemented as a PR (Proportional-Resonant) controller with CCF-AD. Then, step responses of the MPC are compared with different values for the prediction horizon parameters ($N_{p,db}, N_p$) to demonstrate the impact of the parameters on the damping behavior.

The simulations are carried out such that the damping behavior of the controllers at transients can be observed. The LCL-filter system parameters are given in table II. The current reference steps up to the rated current from zero at $t = 0.01$ s, and it steps down at $t = 0.03$ s. The proposed MPC formulation is implemented with an explicit MPC solution ($N_{p,db}=3, N_p=10$). Time-delays due to measurements, computations, and communications are modeled with one sample time delay in

the simulations. The unit-delay method given in [18] is applied to the MPC to compensate the time-delays. As the proposed MPC formulation does not have an internal integrator, small steady-state errors exist. However, this can be overcome by including disturbances in the control model or by shaping the reference currents with compensations [10].

A. Parameter sets in the extended design space

The simulation results for two sets of LCL-filter parameters are shown in fig. 5. The two parameter sets are the ones marked with blue dots in fig. 2(a). Both parameter sets belong to the extended design space, one marked in red and the other marked in yellow, and the results demonstrate the inherent damping capability of MPC in the extended design space. The detailed LCL-filter parameters are given in table II.

In fig. 5(a), the simulation results for the first parameter set are shown, where the LCL-filter has a filter capacitance of $6 \mu\text{F}$ and a resonance frequency directly at the critical resonance frequency (f_{crit}). The PR controller with CCF-AD cannot stabilise the system as discussed in [4] due to resonances, whereas MPC can stabilise the system with good damping and fast transient behaviors.

The simulation results for the second parameter set are shown in fig. 5(b), where the LCL-filter has a filter capac-

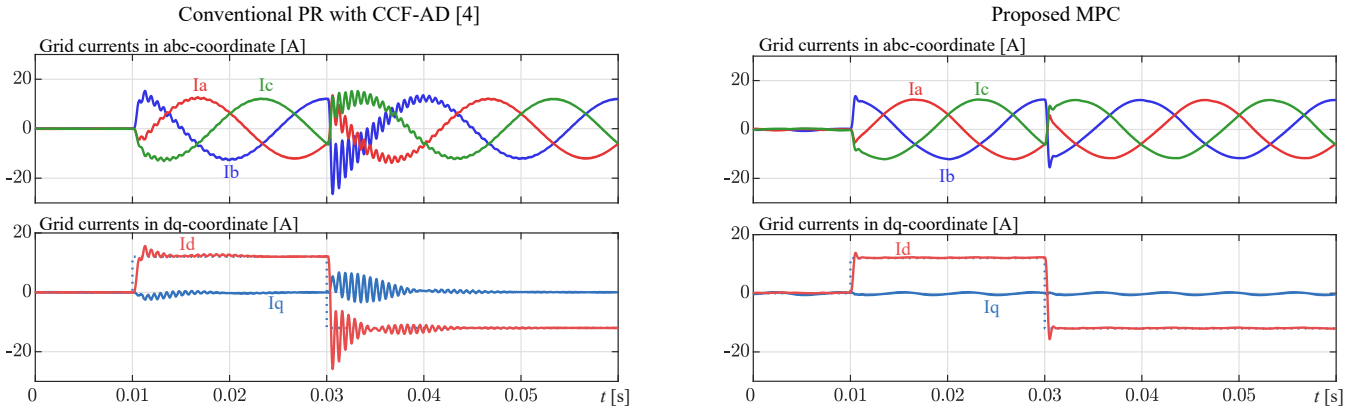


Fig. 6. Simulation result with the parameter set at the optimum point in fig. 2(b). The parameter set belongs to the underdamped group, shown yellow in fig. 2(b), where linear controllers with CCF-AD cannot provide sufficient damping.

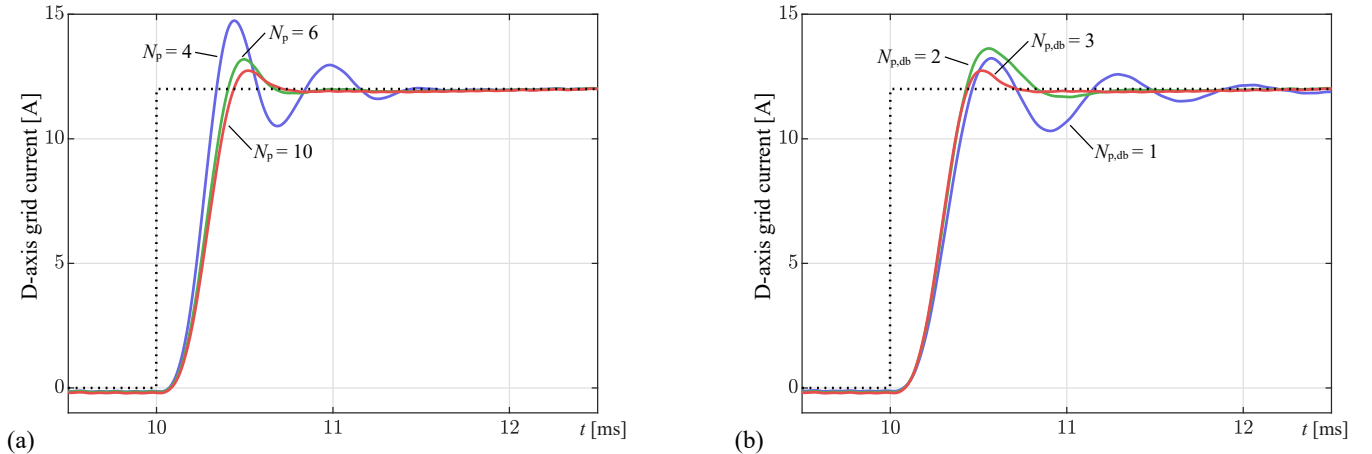


Fig. 7. Comparative simulation results showing the impact of the prediction horizon parameters on the damping of the step response. (a) Impact of N_p (all results with $N_{p,db} = 3$). (b) Impact of $N_{p,db}$ (all results with $N_p = 10$).

itance of $9\ \mu\text{F}$ and a resonance frequency at $1.37\ \text{kHz}$. The corresponding parameter set belongs to the yellow dots in fig. 2(a), indicating that the PR controller with CCF-AD again cannot provide sufficient damping. This can be seen in the results. Oscillations with large overshoots are present for a long period. In contrast, the simulation results with the MPC on the right demonstrate outstanding dynamic control performance with enough damping.

B. Optimum LCL-filter parameter set

The simulation results with the optimum LCL-filter parameter set, which yields the best product of the volume and losses based on the design method in [1], are shown in fig. 6. This parameter set is marked in fig. 2(b) and belongs to the yellow dots, so that the results for the control performance are similar to the one shown in fig. 5(b). Again, the PR controller with CCF-AD cannot provide sufficient damping as expected from the analysis. The simulation results show oscillations with large overshoots over a long period, when the current reference steps are applied. In contrast, the simulation results with the MPC reveal a fast transient behavior with small overshoots.

C. Impact of dead-beat behavior and full prediction horizon

Comparative simulation results are shown in fig. 7 to illustrate the impact of the prediction horizon parameters ($N_{p,db}, N_p$) on the transient and the damping behavior of the MPC. The results with different N_p values are given in fig. 7(a). A longer prediction horizon improves the damping of the step response with the MPC, though the same value of $N_{p,db}$ is used. This is because the MPC can predict the complete resonance response with the long prediction horizon and compute the optimal control inputs to damp the response. With the proposed MPC, the long-prediction horizon is achieved without an excessive increase in computational burden.

The results for different $N_{p,db}$ values are given in fig. 7(b). Similar to the ones above, a longer prediction horizon for a dead-beat behavior improves the damping of the step response with the MPC, though the same value of N_p is used. The dead-beat behavior allows the MPC to fully utilize the dynamics available in the converter for damping the resonance response. However, a bigger $N_{p,db}$ value can result in a larger overshoot because the MPC makes a trade-off between a faster transient behavior and a larger overshoot based on the weighting factors in the cost function.

VII. CONCLUSION

This paper presents an MPC solution to provide sufficient LCL-resonance damping for a wide range of LCL-filter parameters. The wide parameter range has a beneficial impact on the optimal LCL-filter design. The proposed MPC formulation with a smaller number of constraints allows to successfully adopt explicit MPC and enable a real-time implementation even at a high switching frequency. Simulation results with an explicit MPC solution prove the effectiveness of the presented MPC formulation and the inherent damping capability with a long prediction horizon. Exemplary LCL-filter optimization

solutions and the resulting Pareto fronts illustrate possible LCL-filter designs with a trade-off between the volume and the losses. The design sets with MPC achieve lower losses and/or a smaller volume than the design sets with CCF-AD. For exemplary optimum points, which result in the best product of volume and losses, a volume reduction of 43% could be achieved with the proposed MPC by realizing the LCL-filter with the parameters in the extended design space.

REFERENCES

- [1] M. Liserre, F. Blaabjerg, and S. Hansen, "Design and control of an LCL-filter-based three-phase active rectifier," *IEEE Trans. on Industry Applications*, vol. 41, no. 5, pp. 1281–1291, 2005.
- [2] S. Jayalath and M. Hanif, "An LCL-filter design with optimum total inductance and capacitance," *IEEE Trans. on Power Electronics*, vol. 33, no. 8, pp. 6687–6698, 2018.
- [3] J. Dannehl, C. Wessels, and F. W. Fuchs, "Limitations of voltage-oriented PI current control of grid-connected PWM rectifiers with LCL filters," *IEEE Trans. on Industrial Electronics*, vol. 56, no. 2, 2009.
- [4] S. G. Parker, B. P. McGrath, and D. G. Holmes, "Regions of active damping control for LCL filters," *IEEE Trans. on Industry Applications*, vol. 50, no. 1, pp. 424–432, 2014.
- [5] S. Vazquez, J. Rodriguez, M. Rivera, L. G. Franquelo, and M. Norambuena, "Model predictive control for power converters and drives: Advances and trends," *IEEE Trans. on Ind. Electron.*, vol. 64, 2017.
- [6] M. Rossi, P. Karamanakos, and F. Castelli-Dezza, "An indirect model predictive control method for grid-connected three-level neutral point clamped converters with LCL filters," *IEEE Trans. on Industry Applications*, 2022.
- [7] A. Sadie, T. Mouton, M. Dorfling, and T. Geyer, "Model predictive control with space-vector modulation for a grid-connected converter with an LCL-filter," in *Europ. Conf. on Power Electron. and Appl. (EPE ECCE Europe)*, 2019.
- [8] Q. Liu, L. Peng, Y. Kang, S. Tang, D. Wu, and Y. Qi, "A novel design and optimization method of an LCL filter for a shunt active power filter," *IEEE Trans. on Industrial Electronics*, vol. 61, no. 8, 2014.
- [9] Y. Liu, K.-Y. See, S. Yin, R. Simanjorang, C. F. Tong, A. Nawawi, and J.-S. J. Lai, "LCL filter design of a 50-kW 60-kHz SiC inverter with size and thermal considerations for aerospace applications," *IEEE Trans. on Industrial Electronics*, 2017.
- [10] C. Fischer, S. Mariéthoz, and M. Morari, "A model predictive control approach to reducing low order harmonics in grid inverters with LCL filters," in *Conf. of the IEEE Ind. Electron. Soc. (IECON)*, 2013.
- [11] P. Falkowski and A. Sikorski, "Finite control set model predictive control for grid-connected AC–DC converters with LCL filter," *IEEE Trans. on Industrial Electronics*, vol. 65, no. 4, pp. 2844–2852, 2018.
- [12] B. Stöckan, S. Reichert, and M. Diehl, "Model predictive control of a 3-phase grid-connected B6-inverter with LCL-filter in abc-coordinates," in *Europ. Conf. on Power Electron. and Appl. (EPE ECCE Europe)*, 2017.
- [13] A. Gupta, S. Bhartiya, and P. S. Nataraj, "A novel approach to multiparametric quadratic programming," *Automatica*, vol. 47, no. 9, pp. 2112–2117, 2011.
- [14] M. Jeong, S. Fuchs, and J. Biela, "When FPGAs meet regionless explicit MPC: An implementation of long-horizon linear MPC for power electronic systems," in *Conf. of the IEEE Ind. Electron. Soc. (IECON)*, 2020.
- [15] K.-B. Park, F. D. Kieferndorf, U. Drofenik, S. Pettersson, and F. Canales, "Weight minimization of LCL filters for high-power converters: impact of PWM method on power loss and power density," *IEEE Trans. on Industry Applications*, vol. 53, no. 3, 2017.
- [16] J. Mühlethaler, J. W. Kolar, and A. Ecklebe, "Loss modeling of inductive components employed in power electronic systems," in *Intl. Conf. on Power Electron. - ECCE Asia*, 2011, pp. 945–952.
- [17] T. Georgios, "DynACuSo: A high power dynamic arbitrary current source with a modular design," Ph.D. dissertation, ETH Zurich, 2021.
- [18] M. Jeong, S. Fuchs, and J. Biela, "High performance LQR control of modular multilevel converters with simple control structure and implementation," in *Europ. Conf. on Power Electron. and Appl. (EPE ECCE Europe)*, 2020.